



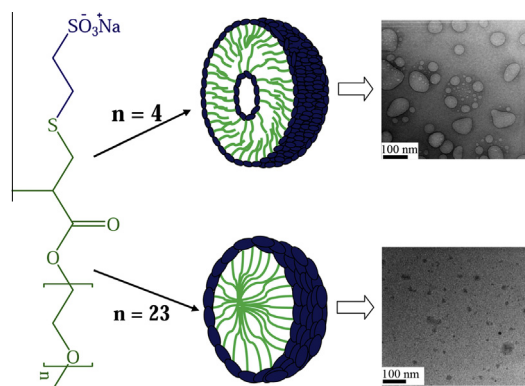
# Aggregation behavior of poly(ethylene glycol) chain-containing anionic amphiphiles: Thermodynamic, spectroscopic and microscopic studies



Rita Ghosh, Joykrishna Dey\*

Department of Chemistry, Indian Institute of Technology Kharagpur, Kharagpur 721302, India

## GRAPHICAL ABSTRACT



## ARTICLE INFO

### Article history:

Received 18 January 2015

Accepted 30 March 2015

Available online 6 April 2015

### Keywords:

Poly(ethylene glycol)

Vesicles

Fluorescence

Microscopy

Isothermal titration calorimetry

## ABSTRACT

Two novel amphiphilic molecules were synthesized by the reaction between poly(ethylene glycol) methyl ether (mPEG) of different chain lengths and sodium-2-mercapto ethane sulfonate (mesna). Different techniques, such as surface tensiometry, conductometry, fluorescence spectroscopy, dynamic light scattering, UV-vis spectroscopy, transmission electron microscopy, and isothermal titration calorimetry were employed to investigate the self-assembly properties of the PEG-based single-tailed amphiphiles in aqueous buffer. Despite having so called polar tail the amphiphiles exhibit aggregate formation in aqueous buffer as well as in water. The shorter chain amphiphile was shown to form bilayer vesicles in contrast to small micelles by its longer chain counterpart. The helicity of the PEG chain was taken into consideration to interpret the difference in self-assembled microstructure formation. The thermodynamics of the self-assemblies were also thoroughly examined. The thermodynamic parameters clearly suggested that the hydrophobic interaction among the PEG chains is the main driving force for aggregate formation. The self-assembled microstructures were observed to be fairly stable with respect to increase of surfactant concentration, aging time and temperature.

© 2015 Published by Elsevier Inc.

## 1. Introduction

Amphiphilic molecules have a general tendency to form organized self-assemblies of different shapes, sizes and morphologies

in solutions above a particular concentration, called critical micelle concentration (*cmc*). The morphology of the self-assemblies formed (spherical and non spherical micelles, worm-like micelles, vesicles, lyotropic liquid crystalline structures, etc.) primarily depends on the molecular structure of the amphiphiles. The aggregate formation is also highly effected by other environmental factors, like surfactant concentration, temperature, pH, ionic strength,

\* Corresponding author. Fax: +91 3222 255303.

E-mail address: joydey@chem.iitkgp.ernet.in (J. Dey).

effect of additives, etc. [1–5]. Formation of aggregate of different shape and morphology due to the change in head-group by keeping the tail fixed has also been reported [6]. The morphology of the aggregates may also vary upon changing the tail keeping the head-group constant. Because of their immense importance in industry, biology, and even in our daily life, surfactants have become the focus of research in the past few decades [7–13].

Poly(ethylene glycol) (PEG) is an important material because of its many fold applications in chemistry, biology, medicinal field and industry. All these versatile properties of PEG arise from its flexible structure, non reactivity, water solubility, and low toxicity. The chemical and biological uses of PEG in surfactant chemistry, drug delivery systems, and osmotic stress techniques are related to the infinitely water-soluble character of the polymers at moderate temperature [14,15]. There are a large number of reports on conformational behavior of the PEG in water and organic solvents. Different techniques like, X-ray [16] (1964), NMR [17] (1965) and IR spectroscopy [18] (1969) showed that the preferred conformations around the C–C and C–O bond of PEG in aqueous solutions were gauche (*g*) and trans (*t*), respectively, suggesting that PEG in aqueous solution preferentially adopts the *tgt* conformation. In 1969, Blandamer et al. [19] reported that water molecules around PEG in aqueous solution form hydrogen bonding (H-bonding) networks similar to that of bulk water on the basis of the distances between oxygen atoms in the *tgt* conformer of PEG and suggested that good fitting of the *tgt* conformer into the hydrogen-bonded networks in the aqueous solution is related to the high solubility of PEG in water. Raman spectroscopic studies [20] and molecular dynamics (MD) studies [21] also implied that PEG in aqueous solution forms helical structure because of the *tgt* conformation in the C–O–C–C–O–C segments. Thus the aqueous behavior of the PEG is truly amazing.

However, for designing an effective drug delivery vehicle, the major issue is that the system must be biocompatible as well as bioavailable. Considering all these factors, PEG was employed for designing the amphiphilic molecules. Here, it should be mentioned that this is not the first report, where PEG has been shown to act as hydrophobic backbone of the amphiphile, there are a few reports from this laboratory on the non-polar character of the PEG [22–24]. But the interesting feature is that we have employed mesna to design the target molecules.

Mesna, which has been used in a variety of disorders, such as a mucolytic agent for pulmonary disorders and as a protective agent against the toxicity of some chemotherapeutic agents, is a synthetic sulfur compound and belongs to a class of thiol compounds that produce mucolysis by disrupting the disulfide bonds of the mucous polypeptide chains [25,26]. Mesna can be used during ear surgeries, such as cholesteatoma or atelectatic ears, to make the dissection of tissue layers simpler [27]. As mesna is hydrophilic in nature it prevents its passage out of the vascular bed into cells. This results in efficient renal clearance and avoids any adverse impact on the cytotoxic effects of ifosfamide. For having such widespread applications of this small molecule in cancer therapy and also in other medical field, mesna was chosen to develop the target amphiphilic molecules. The aim of this work is (i) to design such type of mesna-containing biocompatible amphiphile and (ii) to investigate their solution behavior. Therefore, in this work, two anionic amphiphiles PS1 and PS2 (see Chart 1 for structures) having mPEG tail of different lengths and mesna as the polar head-group were developed. The major objective was to examine if there is any micellization by PS1 and PS2. The aggregation behavior of these amphiphiles was thoroughly investigated in phosphate buffer (20 mM, pH 7.0) at 25 °C. Interfacial properties of the amphiphiles were studied by surface tension method. The *cmc*, micropolarity, and microviscosity of the aggregates were measured by fluorescent probe techniques. The thermodynamics of the self-

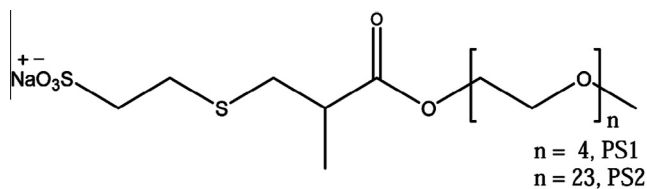


Chart 1. Chemical structures of the amphiphiles.

assembly process was investigated by isothermal titration calorimetry (ITC) through measurements of the standard free energy change ( $\Delta G_m^\circ$ ), standard enthalpy change ( $\Delta H_m^\circ$ ) and standard entropy change ( $\Delta S_m^\circ$ ) of micellization. Dynamic light scattering (DLS) was used to determine the hydrodynamic diameters of the aggregates. The morphology of the aggregates was investigated by use of transmission electron microscopy (TEM). The most interesting result of this work is that the amphiphiles exhibit different aggregation behavior in aqueous buffered solution in spite of having same head group. The difference in morphology of the aggregates formed by these newly developed amphiphiles has been interpreted in terms of the helical nature of PEG chain.

## 2. Materials and methods

### 2.1. Materials

Fluorescence probes, N-phenyl-1-naphthylamine (NPN), pyrene (Py), 1,6-diphenyl-1,3,5-hexatriene (DPH) were purchased from Sigma–Aldrich (Bangalore, India) and were recrystallized from acetone–ethanol mixture at least twice before use. Purity of the probes was confirmed by the fluorescence excitation spectra. Poly(ethylene glycol) methyl ether methacrylate (mPEG; MW 300 and 1100) were obtained from Sigma–Aldrich. Sodium-2-mercapto ethane sulfonate (mesna) was procured from Sigma–Aldrich and was used without further purification. Analytical grade sodium dihydrogen phosphate ( $\text{NaH}_2\text{PO}_4$ ) and disodium monohydrogen phosphate ( $\text{Na}_2\text{HPO}_4$ ) were purchased from SRL, Mumbai. Super dry methanol and super dry triethylamine (TEA) were used for synthesis. Milli-Q water (18 M $\Omega$  cm) was used for the aqueous solution preparation.

The amphiphiles PS1 and PS2 were synthesized by the Michael addition reaction of sodium-2-mercapto ethane sulfonate with poly(ethylene glycol) methyl ether methacrylate by thiol-ene “click” chemistry following reported procedure (Scheme S1, Supporting Information (SI)). The details of the synthesis, chemical identifications, and FT-IR,  $^1\text{H}$ - and  $^{13}\text{C}$  NMR spectra have been presented under SI.

### 2.2. NMR measurements

All 1D and 2D  $^1\text{H}$  NMR spectra were recorded on a Bruker (600 MHz) NMR spectrometer using tetramethyl silane (TMS) as the internal standard spectrometer with  $\text{D}_2\text{O}$  (Aldrich, 99.6 atom % D) solvent as the chemical shift reference for mode locking. To correlate the non-micellar and micellar state of the amphiphile, 0.8 mM (non-micellar) and 8 mM (micellar) solution of PS1 were taken for recording NOESY. Similarly, 0.6 mM (non-micellar) and 5 mM (micellar) solution of PS2 was taken for recording NOESY spectra.

### 2.3. Surface tension measurements

Surface tension ( $\gamma$ ) measurements were performed on a GBX 3S (France) surface tensiometer using Du Nüoy ring method. The

instrument was calibrated and checked by measuring the surface tension of Milli-Q water (18 M $\Omega$  cm) before each experiment. To a 10 mL phosphate buffer (20 mM, pH 7.0) solution, aliquots were added in measured volume and  $\gamma$  (mN/m) was measured in each case. The solution was gently stirred and allowed to equilibrate for 10 min before measurement started. Each measurement was repeated at least three times until the error was within  $\pm 0.01$  mN/m. The temperature of the solution was controlled by a JULABO MC water-circulating bath with a temperature accuracy of  $\pm 0.1$  °C.

#### 2.4. Conductivity measurements

Electrical conductivity ( $\kappa$ ) measurements were performed with a digital conductivity meter (Systronics, model 304) using a conductivity cell of cell constant equal 1.05 cm<sup>-1</sup>. A known volume of the stock solution of PS1 (20 mM) or PS2 (10 mM) in salt-free water was taken in a water-jacketed beaker and  $\kappa$  ( $\mu$ S cm<sup>-1</sup>) was measured at different dilutions of the stock solution at a fixed temperature. The solution was gently stirred magnetically, and the temperature of the solution was controlled by a refrigerated water bath (Lab. Companion, RW-0525GS) with a temperature accuracy of  $\pm 0.1$  °C. After each dilution the solution was equilibrated for 5 min to get a constant conductivity value.

#### 2.5. Steady-state fluorescence measurements

The steady-state fluorescence measurements were performed either on a PerkinElmer LS-55 luminescence spectrometer equipped with a temperature-controlled cell holder or on a Horiba FL3-11 spectrophotometer. A SPEX Fluorolog-3 (model FL3-11) spectrophotometer was used for recording fluorescence emission spectra of Py, NPN, Py, and DPH were used as fluorescence probes to investigate the polarity as well as the viscosity of the microenvironment of the self-assemblies. Surfactant solutions of known concentrations were prepared in pH 7.0 buffer (or water) and were incubated for about 30 min prior to measurement. For fluorescence titration using NPN probe, a saturated solution of NPN in pH 7.0 buffer was used. The final concentration of Py and DPH were kept at 1  $\mu$ M. Py solutions were excited at 335 nm, and emission spectra were recorded in the wavelength range of 350–500 nm using excitation and emission slit widths of 3 and 5 nm, respectively. The solutions containing NPN were excited at 340 nm, and the emission was followed between 350 and 600 nm. The slit width was set at 2.5 nm for excitation and 2.5–10 nm for the emission, depending upon sample concentration. Temperature controlled measurements were carried out by use of a Thermo Neslab RTE-7 circulating bath.

#### 2.6. Fluorescence anisotropy measurements

A PerkinElmer LS-55 luminescence spectrometer was used to measure the steady-state fluorescence anisotropy ( $r$ ) of DPH in presence of the surfactants. The instrument is equipped with a polarization accessory that uses the L-format instrumental configuration and a thermostating and magnetically stirred cell housing that allowed temperature control. The anisotropy was calculated employing the equation:

$$r = (I_{VV} - GI_{VH}) / (I_{VV} + 2GI_{VH}) \quad (1)$$

where  $I_{VV}$  and  $I_{VH}$  are the fluorescence intensities polarized parallel and perpendicular to the excitation light, and  $G (=I_{HV}/I_{HH})$  is the instrumental grating factor. The software supplied by the manufacturer automatically determined the  $G$  factor and  $r$ . For each measurement, the  $r$ -value was recorded over an integration time of 10 s. For each sample, an average of five readings was accepted as

the value of  $r$ . A stock solution of 1 mM DPH was prepared in super dry methanol. Aliquots of this stock solution were added to the surfactant solutions so that the final concentration of the probe was 1  $\mu$ M. The anisotropy measurements were carried out at different surfactant concentrations in the temperature range 25–75 °C. Before measurement started, each solution was equilibrated for 10 min at the experimental temperature. The sample was excited at 350 nm and the emission intensity was followed at 450 nm using excitation and emission slits width of 2.5 nm and 2.5–10.0 nm, respectively. A 430 nm cut-off filter was placed in the emission beam to eliminate the effect of scattered radiation. All measurements started 30 min after sample preparation.

#### 2.7. Time-resolved fluorescence measurements

Optical Building Blocks Corporation EasyLife instrument was employed to measure the fluorescence lifetime of DPH probe. The light source was a 380 nm diode laser. The time-resolved decay curves were analyzed by single exponential or bi-exponential iterative fitting program. The best fit was judged by the  $\chi^2$  value (0.8–1.2) and by the randomness of residual plot.

#### 2.8. Determination of microviscosity

The rigidity or fluidity of the microenvironment of the self-assemblies was measured by determination of the microviscosity ( $\eta_m$ ) using DPH probe. The  $\eta_m$  was calculated from the values of  $r$  and rotational correlation time ( $\tau_R$ ) of DPH probe using Debye–Stokes–Einstein relation [28]:

$$\eta_m = kT\tau_R/v_h \quad (2)$$

where  $v_h$  is the hydrodynamic volume (313 Å<sup>3</sup>) [29] of the DPH molecule. The  $\tau_R$  was calculated using Perrin's equation:

$$\tau_R = \tau_f(r_o/r - 1)^{-1} \quad (3)$$

where  $r_o (= 0.362)$  [30] and  $\tau_f$  are the steady-state fluorescence anisotropy of DPH in a highly viscous solvent and measured fluorescence lifetime of DPH in surfactant solution, respectively.

#### 2.9. Dynamic light scattering

The dynamic light scattering (DLS) measurements were performed with Zetasizer Nano ZS (Malvern Instrument Lab, Malvern, U.K.) light scattering spectrometer equipped with a He–Ne laser operated at 4 mW ( $\lambda_o = 632.8$  nm) at 25 °C. The solution was filtered directly into the thoroughly cleaned scattering cell through a Millipore Millex syringe filter (Triton free, 0.22  $\mu$ m). The sample was allowed to equilibrate inside the DLS optical system chamber for 10 min prior to the start of measurement. The scattering intensity was normally measured at  $\theta = 173^\circ$  to the incident beam. The data acquisition was carried out for at least 15 counts and each experiment was repeated thrice.

#### 2.10. Zeta potential measurements

The surface zeta ( $\zeta$ ) potential of the aggregates were also measured using a Zetasizer Nano ZS (Malvern Instrument Laboratory, Malvern, U.K.) optical system equipped with an He–Ne laser operated at 4 mW ( $\lambda_o = 632.8$  nm) at 25 °C. The measurements were done by taking different surfactant concentrations at 25 °C in pH 7.0 at 25 °C. An average of three successive measurements was noted for each sample.

### 2.11. Transmission electron microscopy (TEM)

The morphology of the aggregates was investigated by a high resolution transmission electron microscope (JEM – 2100 HRTEM, Make – JEOL, Japan) operating at an accelerating voltage of 200 kV. A 4  $\mu\text{L}$  volume of surfactant solution was dropped on to a 400 mesh carbon-coated copper grid, and allowed to stand for 1 min. The excess solution was blotted with a piece of tissue paper, and the grid was air-dried. The specimens were kept in desiccators overnight before measurement. Each measurement was repeated at least twice to check the reproducibility.

### 2.12. Isothermal titration calorimetry (ITC)

A microcalorimeter of Microcal iTC<sub>200</sub>, (made in U.S.A) was used for thermometric measurements. In a microsyringe of capacity 40  $\mu\text{L}$ , 50 mM PS1 and 20 mM PS2 were taken and added in multiple stages to pH 7.0 buffer kept in the calorimeter cell of capacity 200  $\mu\text{L}$  under constant stirring conditions, and the stepwise thermogram of the heats of dilution of the surfactant solution were recorded. The stirring speed was fixed at 400 rpm and pH 7.0 buffer was taken in the reference cell. Each run was duplicated to check reproducibility. Enthalpy calculations were performed with the help of ITC software provided by the manufacturer. All measurements were carried out at 25 °C.

## 3. Results and discussion

### 3.1. Surface activity

The surface properties and interfacial tensions of the amphiphiles at the air/water interfaces were thoroughly investigated by surface tension (ST) measurement. As shown by the plots of  $\gamma$  ( $\text{mN m}^{-1}$ ) vs.  $\log[\text{surfactant}]$  ( $\log C_s$ ) in Fig. 1,  $\gamma$  decreases gradually with the increase of concentration ( $C_s$ ), suggesting spontaneous adsorption of the amphiphiles at the air/water interface. The adsorption efficiency,  $\text{p}C_{20}$  ( $= -\log C_{20}$ , where  $C_{20}$  is the molar concentration of the amphiphile required to reduce  $\gamma$  by 20 units) is much less for both PS1 (2.28) and PS2 (2.36) in comparison to conventional hydrocarbon chain surfactants [31,32]. In fact, the  $\text{p}C_{20}$  values are also less compared to that of structurally similar amphiphile with the zwitterionic L-cysteine head-group [24]. In other words, both PS1 and PS2 were found to be weakly surface-active. This can be attributed to the hydrophilic nature of the PEG chain in comparison to hydrocarbon tail.

It is interesting to note that for both PS1 and PS2 no saturation point could be found in the ST plot even at the highest

concentration employed. However, a small dip (indicated by the downward arrow) in the ST plot is observed at a much lower concentration ( $\sim 2.0$  mM for PS1 and  $\sim 1.0$  mM for PS2) and can be taken as the *cmc* of the amphiphile. The ST plot in the low concentration region has been separately shown as an inset of the corresponding figure. Thus these amphiphiles behave like long-chain fatty alcohols in which the polarity difference between the hydrocarbon chain and  $-\text{OH}$  is very small. The surface behavior of the fatty alcohols (non-electrolyte) in water has been discussed elaborately by Posner et al. [33]. Since the PEG chain of the amphiphiles under investigation is polar relative to the corresponding hydrocarbon chain, both PS1 and PS2 are more soluble in water. At low concentrations the favorable H-bonding interaction between the PEG chain and water molecules causes the PEG tail to lie flat at the air/water interface, resulting in a small decrease of  $\gamma$ -value. Gradual increase of monomer concentration forces the PEG chains to become straight in the interface making more room for other molecules and thus reduces the  $\gamma$ -value. However, for unknown reasons, no sharp break of in the ST plot could be observed in the measured concentration range.

### 3.2. Determination of *cmc*

As the ST plots did not show any saturation point in the investigated concentration range and the amphiphiles are ionic in character, we employed conductivity method to obtain the accurate value of the *cmc*. However, in order to determine *cmc* of the amphiphiles the conductivity ( $\kappa$ ) measurements were performed in water in the absence of any salt at 25 °C. The  $\kappa$  vs.  $C_s$  plots are shown in Fig. 2. As can be seen, a clear break in the plot of both PS1 and PS2 can be observed at a relatively low concentration. The concentration corresponding to the intersection point of the straight lines in the pre- and post-micellar region was taken as *cmc*. The *cmc* values thus obtained are 2.7 and 1.6 mM for PS1 and PS2, respectively. However, as expected this *cmc* value is slightly higher than that obtained from corresponding ST plot. The lower value of *cmc* in phosphate buffer is because of the reduction of ionic repulsion between head groups, which facilitate self-assembly formation. The existence of break-point in the conductivity plot also suggests that the behavior of PS1 and PS2 is similar to that of conventional hydrocarbon chain surfactants and the concentration of free surfactant molecules in the solution remains constant throughout the studied concentration range.

### 3.3. Fluorescence probe studies

Various extrinsic fluorescent probe molecules have been utilized successfully to probe into the microenvironment of the

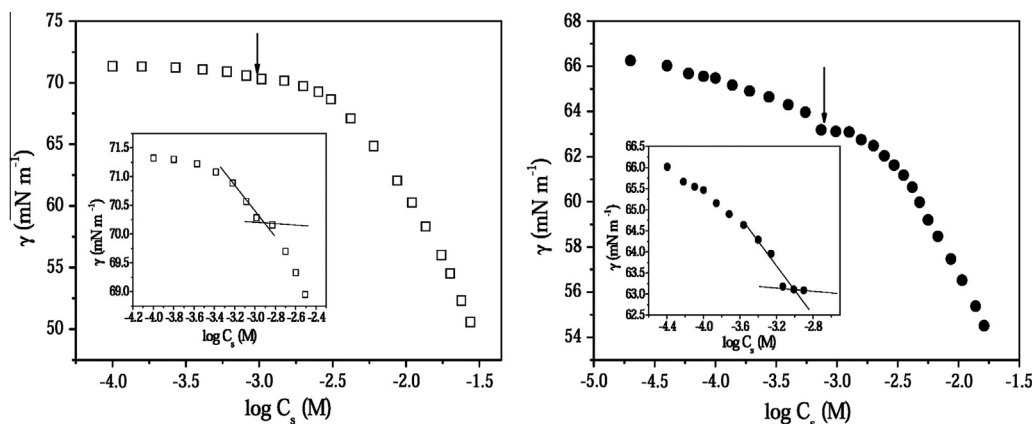
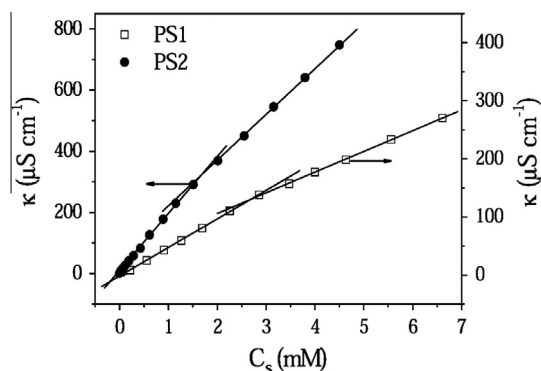
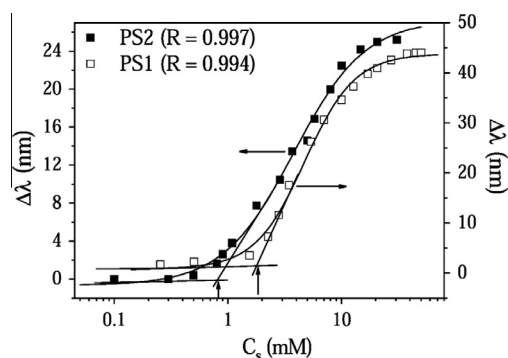


Fig. 1. Plots of variation of surface tension ( $\gamma$ ) as a function of  $\log C_s$  in phosphate buffer (20 mM, pH 7.0) at 25 °C: (□) PS1 and (●) PS2; inset:  $\gamma$  vs.  $\log C_s$  plot in the lower concentration range of the amphiphile.



**Fig. 2.** Plots of conductivity ( $\kappa$ ) versus [surfactant] ( $C_s$ ) in pure water at 25 °C: (□) PS1 and (●) PS2.



**Fig. 3.** Variation of spectral shift ( $\Delta\lambda = \lambda_{\text{water}} - \lambda_{\text{surfactant}}$ ) of NPN probe in phosphate buffer (20 mM, pH 7.0) with the change in  $C_s$  at 25 °C: (□) PS1 and (■) PS2.

aggregates and also to evaluate the *cmc* of surfactants in aqueous solution. In this work, fluorescent probes, such as NPN, Py and DPH were employed to characterize the self-assembly behavior of PS1 and PS2. NPN is a well-known hydrophobic molecule, which is almost insoluble in water, but gets solubilized in the hydrophobic interior of the aggregates. A large spectral shift of the emission maximum ( $\lambda_{\text{max}}$ ) along with a huge rise of fluorescence intensity in the presence of surfactants at concentrations above *cmc* suggests existence of aggregates in aqueous surfactant solution. The blue shift ( $\Delta\lambda = \lambda_{\text{water}} - \lambda_{\text{surfactant}}$ ) is indicative of solubilization of NPN in a less polar environment of the aggregates. The spectral shift was plotted as a function of  $C_s$  as shown in Fig. 3. The *cmc* was determined from the onset of rise of the curve as indicated. The *cmc* thus obtained are 2.0 and 0.9 mM for PS1 and PS2, respectively. The lower value of *cmc* of PS2 must be due to its longer PEG chain. Similar results for structurally similar amphiphile were also reported earlier by this group [24].

In order to confirm aggregate formation in pure water, fluorescence measurements using NPN probe were also performed in

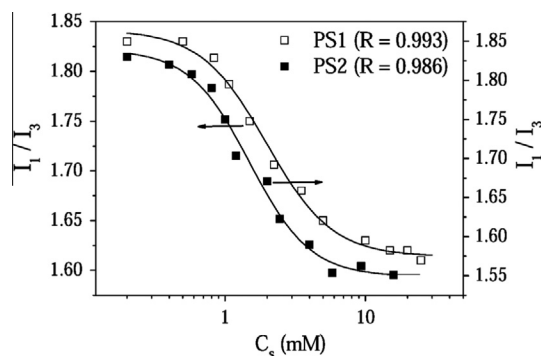


**Fig. 4.** Plots of change in micropolarity index ( $I_1/I_3$ ) with the change in  $C_s$  at 25 °C: (□) PS1 and (■) PS2.

salt-free water. The spectral shift as well as intensity rise confirmed self-assembly formation in water (see Fig. S1 of SI). The corresponding plots of  $\Delta\lambda$  vs.  $C_s$  are depicted in Fig. S2. The *cmc* (3.0 mM for PS1 and 1.9 mM for PS2) as obtained from the respective plot is higher than the corresponding value in phosphate buffer (Table 1). This, as explained earlier, is due to higher ionic strength of the buffer solution that reduces ionic repulsion between head groups and hence *cmc* of the anionic surfactants.

### 3.4. Micropolarity of the self-assemblies

Micropolarity of the self-assemblies was minutely investigated by taking Py as molecular probe. However, the solvent dependent perturbation of the vibronic band intensities has been used to determine the micropolarity and the extent of water penetration into micellar and membrane-like microdomains [34]. In particular, the intensity ratio of the first ( $I_1$ , 374 nm) to the third ( $I_3$ , 384 nm) vibronic band in the Py fluorescence spectrum is typically used as an index of the apparent micropolarity [35]. The  $I_1/I_3$  ratio is, thus, often termed the “micropolarity index”. The fluorescence emission spectra of Py measured in pH 7.0 buffer in the absence and the presence of different concentrations of PS1 and PS2 were depicted and the corresponding Py fluorescence titration plots are shown in Fig. 4. The  $I_1/I_3$  ratio has a value of 1.83 in pH 7.0 buffer in the absence of the surfactant. But the ratio falls off with increasing concentration of the added surfactant and the limiting values become  $1.61 \pm 0.02$  and  $1.56 \pm 0.03$  for PS1 and PS2 respectively, indicating the formation of aggregates with less polar microenvironment [36]. Similar values (Table 1) of  $I_1/I_3$  ratio were also obtained from studies in pure water. This suggests that the polarity of the microenvironment of the self-assemblies is less compared to that of water, but the  $I_1/I_3$  ratio is higher compared to those of conventional surfactants with hydrocarbon tail [31,32]. It should be noted that the micropolarity, within the experimental error limit, is similar for the micelles of both PS1 and PS2. This indicates that the extent of water penetration into the micelle core of both PS1 and PS2 is almost equal.

**Table 1**

The self-assembly properties of PS1 and PS2 in phosphate buffer (20 mM, pH 7.0) at 25 °C; the values within the parentheses correspond to pure water at 25 °C.

Surfactant	pC <sub>20</sub>	<i>cmc</i> (mM)	<i>r</i>	$\eta_m$ (mPa s)	$I_1/I_3$
PS1	2.28	$2.0 \pm 0.1$ ( $3.0 \pm 0.1$ )	$0.174 \pm 0.04^a$ ( $0.162 \pm 0.09^a$ )	$46.0 \pm 3.0^a$ ( $45.0 \pm 5.0^a$ )	$1.61 \pm 0.02^a$ ( $1.63 \pm 0.05^a$ )
PS2	2.36	$0.86 \pm 0.11$ ( $1.9 \pm 0.1$ )	$0.112 \pm 0.07^b$ ( $0.110 \pm 0.12^b$ )	$22.0 \pm 1.5^b$ ( $30.0 \pm 3.0^b$ )	$1.56 \pm 0.03^b$ ( $1.61 \pm 0.06^b$ )

<sup>a</sup> Measured in 40 mM of PS1.

<sup>b</sup> Measured in 20 mM of PS2.

### 3.5. Microviscosity of the self-assemblies

DPH is a well-known membrane fluidity probe, mostly used in the study of lipid bilayer membranes [37]. Steady-state fluorescence anisotropy ( $r$ ) is an index of microviscosity [30] in the vesicle lipidic core. Determination of  $r$  therefore quantifies the rigidity of microenvironment around the DPH probe in the self-assemblies formed by the amphiphiles. Therefore,  $r$  was measured at various concentrations of both PS1 and PS2. The plots in Fig. 5 show the variation of  $r$  with the concentration PS1 and PS2. The fluorescence anisotropy of DPH probe in the self-assemblies of PS2 is similar to those observed with micellar aggregates of conventional anionic surfactants ( $r \sim 0.06$ ) [38]. However, interestingly, the  $r$ -value for self-assemblies of PS1 is relatively higher, suggesting more rigid microenvironment. This can be taken as an indication of the formation of bilayer aggregates by PS1 and small micellar aggregates by PS2. The increase of  $r$  with increasing concentration of PS1 and PS2 can be attributed to the growth of bilayer and micellar aggregates, respectively.

The rigidity of the microenvironments of the self-assemblies can also be quantified by the corresponding microviscosity ( $\eta_m$ ) value. The  $\eta_m$  value, in other words, is an indirect proof of the nature of aggregate type. The  $\eta_m$  values (Table 1) were calculated from

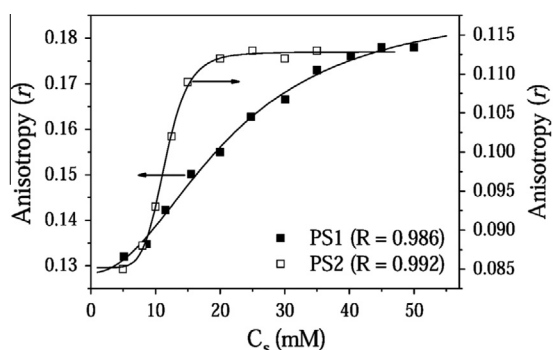


Fig. 5. Plots of anisotropy ( $r$ ) of DPH probe versus concentration of surfactant ( $C_s$ ) at 25 °C: (■) PS1 and (□) PS2.

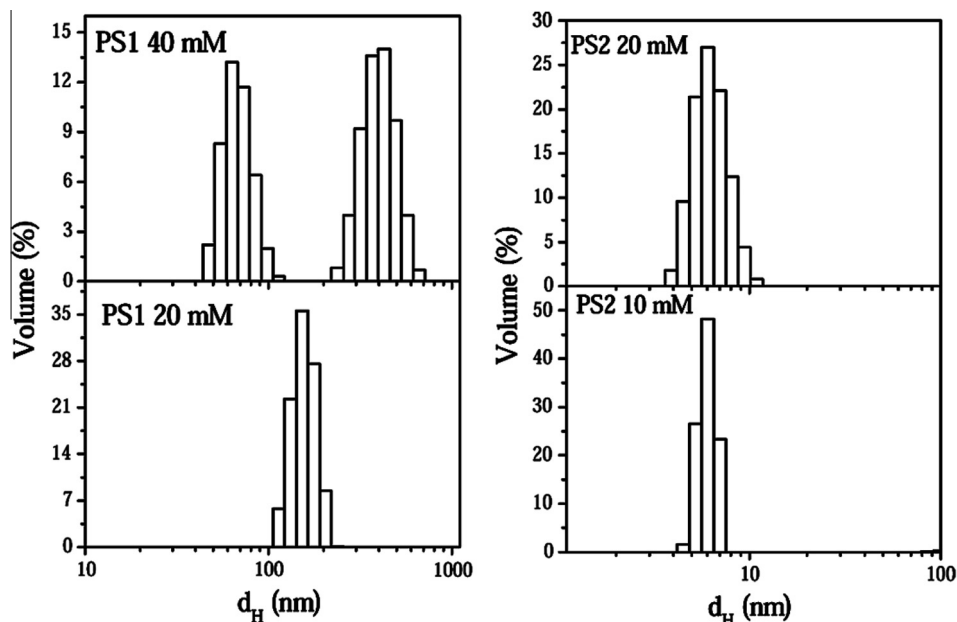


Fig. 6. Size distribution histograms of the aggregates in aqueous buffered solution (20 mM, pH 7.0) of PS1 and PS2 at different concentrations at 25 °C.

the Debye–Stokes–Einstein relation using the steady-state fluorescence anisotropy ( $r$ ) and fluorescence lifetime ( $\tau_f$ ) of DPH probe. The  $\tau_f$  and  $r$  values of the DPH probe were measured in water as well as in phosphate buffer at 25 °C in the presence of known concentration of PS1 (40 mM) and PS2 (20 mM). The data relevant to fluorescence lifetime measurements are included in Table S1 of SI. The longer fluorescence lifetime component of the biexponential decays was used to calculate  $\eta_m$ . For comparison purposes the values of  $r$  and  $\eta_m$  obtained from measurements in water are also included in Table 1. As observed the  $\eta_m$  values of the aggregates in water are similar to those in buffer medium. Relatively larger value of  $\eta_m$  in the case of PS1 (46 mPa s) is consistent with the formation of bilayer aggregates. On the other hand, lower value of  $\eta_m$  in the case of PS2 (22 mPa s) implies micelle formation in buffered solution. It is reported that as the molecular weight of the PEG chain increases (i.e., with the increase in number of ethylene glycol units), the PEG chain becomes helical [39,40]. Thus PS1 having shorter PEG chain spontaneously form larger tightly-packed bilayer aggregates in water as well as in buffered solution, whereas the repulsive interaction among the longer and more helical PEG chain causes the PS2 monomers to form loosely-packed smaller aggregates like micelles. The mutual spatial arrangement of amphiphilic molecules in the aggregated state has been illustrated by the 2D NMR spectra of the molecule as discussed under SI.

### 3.6. Dynamic light scattering (DLS)

The mean hydrodynamic diameter ( $d_H$ ) and size distribution of the aggregates formed by PS1 and PS2 in aqueous buffered solution as well as in pure water was measured by DLS technique. The histograms in Fig. 6 represent the volume distribution graphs of the amphiphiles at different concentrations (for water see Fig. S8). A monomodal size distribution has been observed for PS1 at low concentration, but the concentrated solution exhibits bimodal distributions with  $d_H$  around 40–80 nm and 250–700 nm, suggesting coexistence of aggregates of different sizes. On the other hand, a narrow monomodal distribution with  $d_H$  of around 3–10 nm is observed with PS2, suggesting formation of micellar aggregates in pH 7.0 buffer. The aggregates formed by PS1 with large  $d_H$  values rule out the formation of normal micelles which have diameters

typically in the range of 2–10 nm [41]. Thus the DLS results reveal that despite having same head group and similar tail in the amphiphiles, they show different aggregation behavior in aqueous buffered solution. Similar results were also observed for solutions in pure water. The results are consistent with the conclusions made from fluorescence anisotropy studies. Further the existence of bilayer vesicles in buffered solution of PS1 was confirmed by the TEM measurements as discussed below.

### 3.7. Microstructure of the self-assemblies

In order to visualize the actual shape and size of the microstructures, the HRTEM images (Fig. 7) of the amphiphiles in phosphate buffer were taken. The unstained images of the microstructures in Fig. 7(a and b) clearly exhibit the presence of unilamellar vesicles (ULVs) that enclose an aqueous cavity at both lower and higher concentrations of PS1. Although TEM images obtained by conventional method are often criticized as the method involves drying of the specimen, the images shown in the figure were reproducible. It is clear from the images that in dilute solution, both small (25–60 nm) as well as large vesicles (100–200 nm) are observed with PS1. However, in concentrated solution of PS1, the population of large vesicles (>200 nm) increased, which may be due to fusion of the small vesicles with the larger ones. Unlike PS1, only small (10–15 nm) micellar aggregates are observed in both dilute and concentrated solutions of PS2 (Fig. 7(c and d)). The size of the aggregates of PS1 and PS2 as seen in the TEM images are, however, smaller than that obtained by DLS measurements. This is expected because the former method involved drying of the sample. It should also be noted that aggregates having diameter less than 10 nm could not be observed in the TEM pictures because of limitations of the instrument. However, the diameter of the micelles of PS2 is consistent with its long PEG chain and matches with the value obtained by DLS measurement.

### 3.8. Thermodynamics of self-assembly formation

The micellization behavior of sulfonate head group containing anionic amphiphiles was studied using ITC method at 25 °C. The self-assembly of surfactants in aqueous solution into different types of aggregates is a widely studied phenomenon and many techniques have already been utilized to explore this process. Among them ITC has mostly been employed [42–44], as it is capable of determining directly the *cmc* and the heat of micellization ( $\Delta H_m^\circ$ ) in single titration. The process is done by diluting a micellar surfactant solution into water at a fixed temperature. From this calorimetric titration curve, the *cmc* and  $\Delta H_m^\circ$  values can be directly obtained from the inflection point of the respective plot and from the enthalpy difference between final and initial enthalpies, respectively. The other thermodynamic parameters,  $\Delta G_m^\circ$  and  $\Delta S_m^\circ$  associated with the micellization process can be calculated using pseudophase separation model [43]. The *cmc* values and the

respective heat of dilution have been evaluated from Fig. 8 and are collected in Table 2. The positive  $\Delta H_m^\circ$  values for both PS1 and PS2 emphasized that the aggregate formation whether it is micelle or vesicle, is endothermic in nature. The  $\Delta G_m^\circ$  values were found to be highly negative, which imply spontaneity of the aggregate formation. However, the aggregate formation is less favored in the case of PS1 which might be due to relatively more polar and short PEG chain. The  $T\Delta S_m^\circ$  value calculated from the respective  $\Delta S_m^\circ$  value is observed to be much higher than that of corresponding  $\Delta H_m^\circ$  value. That is the aggregate formation by both amphiphiles is found to be entropy-driven. In fact, hydrophobic interaction is the sole criteria of entropy-driven processes, such as micelle formation [45]. Thus, the hydrophobic interaction among PEG chains into the micellar interior drives the process of micellization as in the case of hydrocarbon chain containing conventional surfactants, in which the hydrocarbon tails accumulate by hydrophobic interaction to give micellar aggregates. This implies that the thermodynamics behind aggregate formation are similar for both PEG containing amphiphiles and hydrocarbon tail containing surfactants. Interestingly, despite having more polar PEG chain the PS1 favors vesicle formation in contrast to micelles formed by PS2. This may be attributed to the more helical nature of the PEG chain in the case of PS2.

### 3.9. Aggregate stability

Once we confirmed the formation of vesicles by, the next objective was to examine their stability. The stability of the self-assemblies was therefore investigated under various physical conditions including time, temperature, surface charge, and additives, emphasizing the stability of the spontaneously formed vesicles and their ability of incorporation and exemption of drugs and other biomedical applications.

#### 3.9.1. Zeta potential

In order to estimate the surface charge of the aggregates at different concentrations,  $\zeta$ -potential measurements of the buffered solutions of PS1 and PS2 were performed. A high  $\zeta$ -potential value (positive or negative) indicates system's stability against flocculation or coagulation. Relatively high  $\zeta$ -potential values are expected for the amphiphiles with sulfonate head group. The  $\zeta$ -potential values of the vesicular and micellar aggregates of PS1 and PS2, respectively are listed in Table S2 of SI. As expected, the negative charge density is high for both types of aggregates formed by PS1 and PS2. Because of intermolecular repulsive interactions among the large sulfonate head groups, the vesicles of PS1 are expected to be sufficiently stable. This is manifested by the results of aging effect.

#### 3.9.2. Aging effect

In order to investigate the stability of the aggregates, the turbidity ( $\tau = 100 - \% T$ ) of the amphiphile solution was measured at different time intervals. Generally, turbidity arises from the scattering

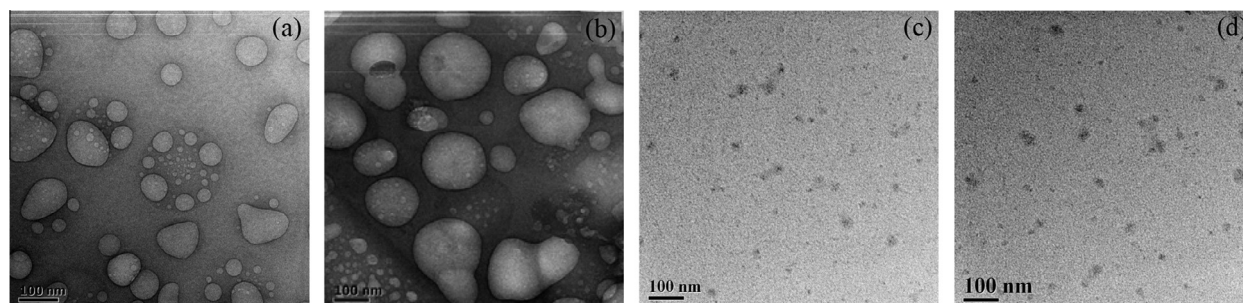


Fig. 7. HRTEM micrographs of (a) 10 mM PS1, (b) 20 mM PS1, (c) 5 mM PS2 and (d) 10 mM PS2 solutions.

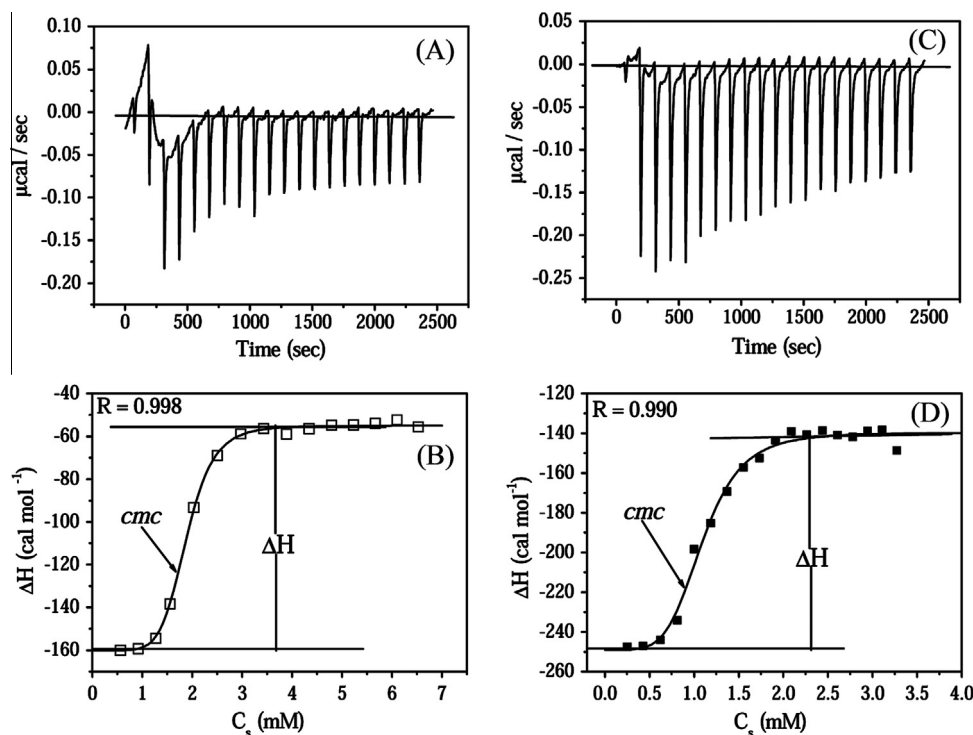


Fig. 8. Calorimetric traces (heat flow against time) for PS1 (A) and PS2 (C), and variation of enthalpy change with  $C_s$  for PS1 (B) and PS2 (D).

Table 2

Critical micelle concentration ( $cmc$ ), standard Gibbs free energy change ( $\Delta G_m^\circ$ ), standard enthalpy change ( $\Delta H_m^\circ$ ) and standard entropy change ( $\Delta S_m^\circ$ ) of the micelle formation in phosphate buffer (20 mM, pH 7.0) of PS1 and PS2 at 25 °C.

Surfactant	$cmc$ (mM)	$(\Delta G_m^\circ)$ (kJ mol <sup>-1</sup> )	$(\Delta H_m^\circ)$ (kJ mol <sup>-1</sup> )	$(\Delta S_m^\circ)$ (J K <sup>-1</sup> mol <sup>-1</sup> )	$T(\Delta S_m^\circ)$ (kJ mol <sup>-1</sup> )
PS1	2.6 (±0.1)	-14.66	0.27 (±0.06)	50.09	14.93
PS2	1.0 (±0.2)	-16.99	0.43 (±0.09)	58.50	17.43

of light by the dispersed vesicles or micelles, and depends on their sizes and populations. The turbidity of 10 mM PS1 and 5 mM PS2 in pH 7.0 (20 mM) buffer was monitored at 400 nm at different time intervals during 30 days. The experimental results are presented in Fig. S9 of SI. The plot reveals that the turbidity initially increases only slightly with time, and reaches almost a steady value. The initial increase in turbidity could be attributed to the formation and growth of vesicles (PS1) or micelles (PS2) upon aging, while the subsequent plateau refers to the storage life of the aggregates.

### 3.9.3. Thermal stability of the self-assemblies

Determination of physical stability of micelles and vesicles at higher temperatures is necessary for their practical applications and therefore, the effect of temperature on their stability was also studied. The fluorescence anisotropy of DPH probe solubilized in the vesicle bilayer was monitored in the temperature range of 25–75 °C. Fig. 9(a) shows the variation of  $r$  with temperature of a 40 mM PS1 and a 20 mM PS2 solution. The magnitude of  $r$  is higher at low temperature, but it decreases with the increase in temperature. This is because the viscosity of the microenvironment decreases with the rise in temperature due to weakening of the hydrophobic interaction and other physical forces among PEG chains that are responsible for forming the aggregates. In the case

of vesicles of PS1, this causes phase transition of the bilayer membrane from more rigid gel state to a more fluid liquid-crystalline state. Thus the temperature corresponding to the inflection point of the sigmoidal curves can be taken as the phase transition temperature,  $T_m$ . The higher value of  $T_m$  (44 °C) is consistent with the stronger interactions among PEG chains in the vesicle bilayer of PS1. As indicated by the value of  $r$  (0.155), the vesicle structure still remains at 75 °C. This is also confirmed by the size distribution histogram and corresponding TEM image of the vesicle solution at 75 °C as shown in Fig. 9(b and c). Clearly the vesicles of PS1 are quite stable at the physiological temperature (37 °C) and therefore can be used for drug delivery purposes. On the other hand, in the case of PS2, the interaction among PEG chains being weak the micelles get disrupted as a result of increase of temperature above 49 °C.

### 3.9.4. Effect of additives

The effect of salt concentration on the aggregation behavior of PS1 and PS2 was also systematically studied. It is commonly observed that the increase of counter ion concentration or even an increase of ionic strength of ionic surfactant solution induces transition of bilayer vesicles to form spherical micelles and rod-like micelles [46], tubular structure [47] or from small vesicles to giant vesicles [48]. In order to examine this, the fluorescence anisotropy ( $r$ ) of DPH probe was monitored by taking 40 mM PS1 and 20 mM PS2 with the variation of the concentration of three types of salts, such as NaCl, choline chloride, and L-lysine having different cations. It was observed that, the additives had no significant effect on the fluorescence anisotropy of DPH in the small micelles of PS2, suggesting either micellar structures remain unchanged or undergo transition to form larger micelles. Addition of salt causes the reduction of electrostatic repulsion among the anionic head-groups which results in a growth of aggregates. However, absence of any increase in viscosity of the solution ruled out the possibility of formation of large rod-like aggregates. Similar to micellar structures of PS2, the increase of NaCl concentration also did not show

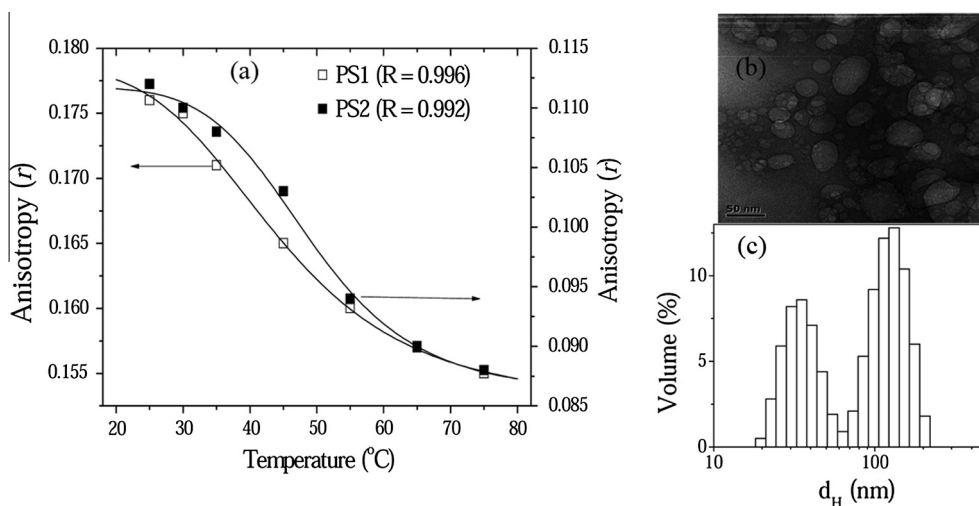


**Fig. 9.** (a) Plots showing variation of fluorescence anisotropy ( $r$ ) of DPH probe in 40 mM PS1 and 20 mM PS2 solution with temperature (°C); representative TEM micrograph (b), and size distribution histograms (c) of 40 mM PS1 solution at 75 °C.

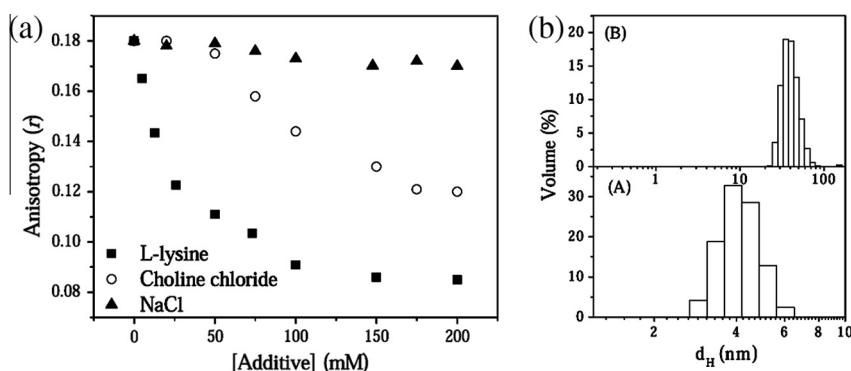


**Fig. 10.** (a) Variation of fluorescence anisotropy ( $r$ ) of DPH probe in 40 mM PS1 with the concentration of NaCl ( $\blacktriangle$ ), L-lysine ( $\blacksquare$ ) and choline chloride ( $\circ$ ); (b) size distribution histograms (c) of 40 mM PS1 solution in the presence of 150 mM L-lysine (A) and 200 mM choline chloride (B).

any significant change in fluorescence anisotropy of DPH in the bilayer vesicles of PS1 (Fig. 10(a)). However, the vesicle size was observed to increase upon addition of NaCl (Fig. S10). Interestingly, addition of organic salts, such as choline chloride and L-lysine was observed to have a significant effect on the stability of the vesicles of PS1. The plot of  $r$  of DPH probe in 40 mM PS1 as a function of [L-lysine] or [choline chloride] has been depicted in Fig. 10(a). For both L-lysine and choline chloride, the plot shows a sharp decrease of  $r$  with the increase of additive concentration, suggesting transformation of bilayer structure to some other morphology. The transformation of the vesicles to small vesicles in the presence of choline chloride is shown by the corresponding size distribution histogram in Fig. 10(b). However, when L-lysine was added the vesicular structures of PS1 are transformed into small micelles with  $d_H$  of about 4 nm. The increased salt concentration, however, reduces the surface charge density of the aggregates as indicated by the reduction of  $\zeta$ -potential (see Fig. S11). The different effects of L-lysine and choline chloride on the vesicular structures of PS1 can be attributed to the difference in polarity of the organic counter ions. In the case of choline chloride, the cation is more hydrophobic than that of L-lysine. Thus relatively weak electrostatic interaction of choline chloride with the  $-\text{SO}_3^-$  head group and steric hindrance following its solubilization in the bilayer causes partial disruption of the vesicles, leading to the formation of smaller vesicles. On the other hand, relatively strong interaction of the L-lysine cation with the  $-\text{SO}_3^-$  head group results in a

complete destruction of PS1 vesicles forming small micellar aggregates as shown by the size distribution histograms in Fig. 10(b).

#### 4. Conclusions

In conclusion, we have designed and synthesized two novel mesna based amphiphiles with PEG as hydrophobic tail. We have investigated the surface activity and intriguing self-assembly properties of the amphiphiles in buffer (pH 7.0). Unlike conventional fatty acid surfactants with hydrocarbon tail [29,30], these amphiphiles showed weak surface activity at the air/water interface. However, the  $cmc$  of these amphiphiles is relatively low. On the basis of the experimental results of fluorescence, DLS and TEM measurements PS1 with shorter PEG chain was observed to have strong tendency to self-organize spontaneously to form stable unilamellar vesicles in dilute as well as in concentrated solutions, whereas small micellar aggregates were observed to form in both dilute and concentrated solutions of PS2 bearing longer PEG chain. The difference in aggregation behavior of the PEG based amphiphiles having same head group has been attributed to the difference in conformation of the PEG chain. The helicity of the PEG chain turns out to be the main reason for different self-assembled microstructure formation in the aggregated state. The longer PEG chain of PS2 amphiphile has been shown to be helical in nature. Although the bilayer membranes of the vesicles of PS1 surfactant

is more rigid, but the micropolarity of the aggregates of both PS1 and PS2 is higher than that of normal micelles of hydrocarbon surfactants [29,30]. The thermodynamics of aggregate formation, however, was observed to be very similar to conventional surfactants [42,43]. The large positive values of  $\Delta S_m^\circ$  indicated that the driving force behind the spontaneous aggregate formation is hydrophobic interaction [45]. A similar aggregation behavior of both anionic [22] and cationic [23] surfactants containing PEG tail has already been reported by our group. While the amphiphiles with the same PEG tail but carboxylate head-group is observed to form disk-like aggregates [22], the surfactants employed in this work forms either vesicles or micelles. The aggregate morphology of PS1 is similar to that of structurally similar amphiphiles mPEG<sub>300</sub>-Cys and mPEG<sub>1100</sub>-Cys with a zwitterionic head-group (L-cysteine) [24]. Interestingly, unlike PS1 and PS2 with sulfonate as head-group when the head-group is L-cysteine, the aggregation behavior is independent of PEG chain length. The vesicles as well as the micelles formed by the PS1 and PS2 surfactants were also observed to be sufficiently stable at the physiological temperature for a longer period of time which suggests that they could have potential use in drug delivery. The addition of choline chloride caused transformation of the large vesicles of PS1 into smaller vesicles. However, the vesicular aggregates transformed into small micellar aggregates in the presence of relatively low concentration of L-lysine.

#### Acknowledgments

The authors thank Indian Institute of Technology, Kharagpur for financial support of this work. We are thankful to Prof. N. Sarkar for the DLS and zeta potential measurements.

#### Appendix A. Supplementary material

Supplementary data associated with this article can be found, in the online version, at <http://dx.doi.org/10.1016/j.jcis.2015.03.054>.

#### References

- [1] J.H. Fuhrhop, W. Helfrich, *Chem. Rev.* 93 (1993) 1565–1582.
- [2] M. Johnsson, A. Wagenaar, B.F.N.J. Engberts, *J. Am. Chem. Soc.* 125 (2003) 757–760.
- [3] M. Bergsma, L.M. Fielden, B.F.N.J. Engberts, *J. Colloid Interface Sci.* 243 (2001) 491–495.
- [4] L. Jiang, K. Wang, M. Deng, Y. Wang, J. Huang, *Langmuir* 24 (2008) 4600–4606.
- [5] S.T. Davies, M.A. Ketner, R.S. Raghavan, *J. Am. Chem. Soc.* 128 (2006) 6669–6675.
- [6] A. Mohanty, J. Dey, *Langmuir* 23 (2007) 1033–1040.
- [7] L.M. Rodrigues, I. Banat, J. Teixeira, R. Oliveira, *J. Antimicrob. Chemother.* 57 (2006) 609–618.
- [8] D. Kitamoto, T. Morita, T. Fukuoka, M. Konishi, T. Imura, *Curr. Opin. Colloid Interface Sci.* 14 (2009) 315–328.
- [9] I.L. Jacob, A.C. Nuncs, A. Bosc, *J. Colloid Interface Sci.* 168 (1994) 289–301.
- [10] Y. Sumida, A. Masuyama, M. Takasu, T. Kida, Y. Nakatsuji, I. Ikeda, M. Nojima, *Langmuir* 17 (2001) 609–612.
- [11] X. Guo, F.C. Szoka Jr., *Acc. Chem. Res.* 36 (2003) 335–341.
- [12] D. Zhi, S. Zhang, S. Cui, Y. Zhao, Y. Wang, D. Zhao, *Bioconjugate Chem.* 24 (2013) 487–519.
- [13] D. Felnerova, J.F. Viret, R. Glück, C. Moser, *Curr. Opin. Biotechnol.* 15 (2004) 518–529.
- [14] D.L. Elbert, J.A. Hubbell, *Annu. Rev. Mater. Sci.* 26 (1996) 365–394.
- [15] S. Dhawan, K. Dhawan, M. Varma, V.R. Sinha, *Pharm. Technol.* 29 (2005) 82–96.
- [16] H. Tadokoro, Y. Chatani, T. Yoshihara, S. Murahashi, *Makromol. Chem.* 73 (1964) 109–127.
- [17] T.M. Connor, K.A. McLaughlan, *J. Phys. Chem.* 69 (1965) 1888–1893.
- [18] K. Liu, J.L. Parsons, *Macromolecules* 2 (1969) 529–533.
- [19] M.J. Blandamer, M.F. Fox, E. Powell, J.W. Stafford, *Makromol. Chem.* 124 (1969) 222–231.
- [20] J.L. Koenig, A.C.J. Angood, *Polym. Sci. Part A* 8 (1970) 1787–1796.
- [21] K. Tasaki, *J. Am. Chem. Soc.* 118 (1996) 8459–8469.
- [22] J. Dey, S. Shrivastava, *Soft Matter* 8 (2012) 1305–1308.
- [23] J. Dey, S. Shrivastava, *Langmuir* 28 (2012) 17247–17255.
- [24] R. Ghosh, J. Dey, *Langmuir* 30 (2014) 13516–13524.
- [25] S.W. Clarke, M.T. Lopez-Vidriero, D. Pavia, *Br. J. Clin. Pharmacol.* 7 (1979) 39–44.
- [26] M. Berrigan, A. Marinello, Z. Pavelic, *Cancer Res.* 42 (1982) 3688–3695.
- [27] M. Yilmaz, N. Goksu, I. Bayramoglu, *ORL J. Otorhinolaryngol. Relat. Spec.* 68 (2006) 195–198.
- [28] J.R. Lakowicz, *Principles of Fluorescence Spectroscopy*, Plenum Press, New York, 1983, p. 132.
- [29] S. Roy, A. Mohanty, J. Dey, *Chem. Phys. Lett.* 414 (2005) 23–27.
- [30] M. Shinitzky, Y. Barenholz, *J. Biol. Chem.* 249 (1974) 2652–2657.
- [31] A. Mohanty, J. Dey, *Langmuir* 20 (2004) 8452–8459.
- [32] T. Patra, S. Ghosh, J. Dey, *Soft Matter* 6 (2010) 3669–3679.
- [33] A.M. Posner, J.R. Anderson, A.E. Alexander, *J. Colloid Sci.* 7 (1952) 623–644.
- [34] B.L. Hammouda, D. Ho, S. Kline, *Macromolecules* 37 (2004) 6932–6937.
- [35] K. Kalyansundaram, *Photophysics of Microheterogeneous Systems*, Academic Press, New York, 1988.
- [36] K. Kalyansundaram, J.K. Thomas, *J. Am. Chem. Soc.* 99 (1977) 2039–2044.
- [37] E.D. Cehelnik, R.B. Cundall, J.R. Lockwood, T.F. Palmer, *J. Phys. Chem.* 79 (1975) 1369–1376.
- [38] R. Zana, I. Martin, H. Lévy, *Langmuir* 13 (1997) 5552–5557.
- [39] R. Wada, K. Fujimoto, M. Kato, *J. Phys. Chem. B* 118 (2014) 12223–12231.
- [40] A. Maestre, P. Guardado, M. Luisa Moya, *J. Chem. Eng. Data* 59 (2014) 433–438.
- [41] A. Jusufi, A.P. Antti-Pekka Hynninen, M. Haataja, A.Z. Panagiotopoulos, *J. Phys. Chem. B* 113 (2009) 6314–6320.
- [42] S. Paula, W. Siis, J. Tuchtenhagen, A. Blume, *J. Phys. Chem.* 99 (1995) 11742–11751.
- [43] P. Majhi, S. Moulik, *Langmuir* 14 (1998) 3986–3990.
- [44] P. Garidel, A. Hildebrand, R. Neubert, A. Blume, *Langmuir* 16 (2000) 5267–5275.
- [45] D.P. Ross, S. Subramanian, *Biochemistry* 20 (1981) 3096–3102.
- [46] A. Mohanty, T. Patra, J. Dey, *J. Phys. Chem. B* 111 (2007) 7155–7159.
- [47] T. Lu, F. Han, Z. Li, J. Huang, *Langmuir* 22 (2006) 2045–2049.
- [48] I. Grillo, E.I. Kats, A.R. Muratov, *Langmuir* 19 (2003) 4573–4581.